Online Research @ Cardiff

This is an Open Access document downloaded from ORCA, Cardiff University's institutional repository: https://orca.cardiff.ac.uk/id/eprint/111081/

This is the author's version of a work that was submitted to / accepted for publication.

Citation for final published version:

Townsend, Scott, Picelli Sanches, Renato, Stanford, Bret and Kim, Hyunsun ORCID: https://orcid.org/0000-0002-5629-2466 2018. Structural optimization of plate-like aircraft wings under flutter and divergence constraints. AIAA Journal 56 (8) , pp. 3307-3319. 10.2514/1.J056748 file

Publishers page: https://doi.org/10.2514/1.J056748 <https://doi.org/10.2514/1.J056748>

Please note:
Changes made as a result of publishing processes such as copy-editing, formatting and page numbers may not be reflected in this version. For the definitive version of this publication, please refer to the published source. You are advised to consult the publisher's version if you wish to cite this paper.

This version is being made available in accordance with publisher policies. See http://orca.cf.ac.uk/policies.html for usage policies. Copyright and moral rights for publications made available in ORCA are retained by the copyright holders.

information services
gwasanaethau gwybodaeth

Structural Optimization of Plate-Like Aircraft Wings under Flutter & Divergence Constraints

Scott Townsend[1] and Renato Picelli[2]
Cardiff University, Cardiff, CF24 3AA, UK

Bret Stanford[3]
NASA Langley Research Center, Hampton, VA, 23681, USA.

H. Alicia Kim[4]
UC San Diego, CA, 92093, USA and Cardiff University, Cardiff, CF24 3AA, UK

Minimum-weight aircraft wing design, with an emphasis on avoiding aeroelastic instability, has been studied since the 1960's. The majority of works to date were posed as sizing problems; only a handful of researchers have employed a topology optimization approach. The aim of this study is to utilize the level set method for this purpose: The problem is formulated as one of plate thickness distribution, which takes on one of two prescribed values at every point on the wing planform. We combine this with constraints implemented on the eigenvalues of the flutter equation; such an approach is shown to be robust and versatile. We include optimization results for rectangular plate wings at a range of sweep configurations studied previously in order to validate our methods. We then optimize delta, high aspect ratio and typical swept transport wing planforms. All solutions demonstrate the ability to significantly reduce wing mass while maintaining flutter and divergence speed above a specified limit, which can be higher than that of the reference, maximum-thickness design. We submit that the proposed method can be used to provide insights into optimal aeroelastic wing structures, particularly useful for developing unconventional aircraft

---

[1] Postdoctoral Research Associate, School of Engineering, townsends3@cf.ac.uk
[2] Postdoctoral Research Associate, School of Engineering, picellir@cf.ac.uk
[3] Research Aerospace Engineer, Aeroelasticity Branch, bret.k.stanford@nasa.gov, AIAA Senior Member.
[4] Professor, Department of Structural Engineering, alicia@ucsd.edu, AIAA Associate Fellow.

structural configurations.

Nomenclature

$[M]$	= mass matrix
$[C]$	= structural damping matrix
$[K]$	= stiffness matrix
$[Q] \equiv [Q]' + i\,[Q]''$	= aerodynamic pressure matrix
$[F]$	= flutter equation matrix
$\{u\}$	= deflection of structure
$p \equiv \gamma + ik$	= eigenvalue of flutter equation
ρ	= air density
V	= air speed
$q = \frac{1}{2}\rho V^2$	= dynamic pressure
c	= chord length
V_f	= flutter airspeed
V_d	= divergence airspeed
$V_c \equiv \min(V_f, V_d)$	= critical airspeed
f_c	= fraction of critical airspeed
W	= weight, expressed as proportion of wing area
ϕ	= level set function
$H(.)$	= Heaviside operator
$\delta(.)$	= Kronecker delta operator
Ω	= structure topology i.e. plate thickness distribution

I. Introduction

In many areas of engineering, topology optimization methods have produced designs often radically-different from those suggested by intuition alone. Weight reductions of 20% and more

are routinely achieved in the automotive industry, prompting a representative to remark: "Topology and shape optimization have become the most important development tools used by the Audi AG in the last few years" [1].

The above notwithstanding, sparse is the literature regarding its application in aircraft aeroelasticity. This is not to say that a broader class of optimization methods are not frequently and successfully applied in this field. Indeed, there has been great interest since the 1960's in developing algorithms to minimize the weight of an aircraft subject to constraints on its aeroelastic performance. This so-called aeroelastic tailoring has since facilitated numerous developments in high-performance aircraft design, perhaps most notably the forward-swept wings of the X-29 demonstrator aircraft, wherein divergence is prevented via judicious distribution of composite thickness and fiber orientation [2].

The established aeroelastic design tools such as `TSO` [3] and `ASTROS` [4], as well as the vast majority of works found in the literature, formulate the design problem as one of sizing: A wing structural layout is assumed a priori, the parameters of which are then optimized in a continuous fashion. Numerous works have centered on the thickness distribution of plates within a fixed planform, either that of wings modeled as such [5–7], or of the skin fastened over a three dimensional wing structure [8–10]. Composite lamination parameters [11], ply orientation [9], and plate material properties [12] have likewise comprised the design variables in optimization studies. Using such sizing formulations, one retrieves a design with, for example, a continually-varying skin thickness distribution. From perspectives such as physical interpretation or manufacturability, one may, in contrast, prefer binary designs, whereby skin thickness is constrained to take on one of several allowed values; such is the essence of topology optimization methods, and formed the primary motivation for this work.

As noted above, flutter and/or divergence-based topology optimization studies are rare though not entirely absent. Stanford et al [13] optimized rectangular, plate-like wings at several different sweep configurations via an unconstrained, weighted objective function, comprised of wing mass and critical speed (defined herein as the minimum of the flutter and divergence speeds), with additional penalty terms to force binary plate thickness. This early work suggested that "the use of

a variable-thickness topology optimization can consistently locate designs that outproduce uniform thickness plates in a multi-objective sense: higher flutter/divergence speeds, lighter weight" [13]. Furthermore, rib and spar structures have been subjected to topology optimization methods [14]: The outer mold line of a common research model (CRM) wing was populated with a fixed lattice of orthogonal ribs and spars, each of which were subsequently designed to maximize flutter speed. The retrieved structures were far from typical, and accorded significant changes in both flutter mode shape and dynamic pressure when compared to the initial design. Common to these works was the incorporation of aeroelastic metrics (flutter speed, etc.) in the objective function, rather than as constraints; such is more commonly encountered in the aforementioned sizing optimization studies, wherein two main approaches are prevalent: Enforcing a single constraint on the flutter speed [5], and constraining the eigenvalues of the flutter equation directly. The former is computationally more efficient, the latter avoids issues associated with discontinuities in flutter and divergence speed with respect to design changes [8].

The constrained formulation is at least as useful in practice as the unconstrained one, and in general, the two will conclude different optima. It thus stands to reason that topology-optimized wing structures remain to be uncovered. Most recently, Dunning et al employed the constrained topology optimization approach to the entire interior of a CRM wing [15]. Such a strategy proved effective at obtaining feasible optimal designs, though it is noted that the choice of initial design appeared most influential over the retrieved optima, necessitating further studies.

In light of the above, we herein present a further investigation of flutter and divergence-constrained topology optimization methods. In order to maintain relative simplicity in analysis and interpretation of results, this work will focus on plate-like aircraft wings: Our goal will be to obtain the optimal plate thickness distribution over a given wing planform; such can be interpreted as the design of stiffening elements in a wing [16]. In contrast to Stanford and Beran [13], we employ a constrained optimization, and also favor a level set topology optimizer which will be shown to obtain superior wing topologies compared to those obtained with the intermediate-density approach of Ref. [13]. This work considers the rectangular planforms considered in Ref. [13], as well as delta, high aspect ratio and typical swept transport wing planforms. Section II introduces the flutter

equation and its use in predicting the aeroelastic behavior of plate-like wings. Section III describes the level set method and its role in distributing plate thickness in an optimal fashion. Section IV details our method of constraint-handling, and includes the derivation of constraint sensitivity with respect to design variables. Section V provides optimization results for the range of considered planforms. We conclude in Section VI.

II. Simulation Method

The flutter equation relates the dynamic aerodynamic loading on a structure to its deformation, and can be written in discrete form as (see, e.g. [4, 17]):

$$\left[\left(\frac{2V}{c}\right)^2 p^2 M + \left(\frac{2V}{c}\right) pC + K - q\left(Q'(k) + \frac{p}{k}Q''(k)\right)\right]\{u\} \equiv [F]\{u\} = \{0\} \tag{1}$$

We calculate the aerodynamic loading matrices $[Q] \equiv [Q]' + i[Q]''$ via the doublet-lattice method, using 4-node surface elements with a quartic approximation to the Kernel function [18]. The structural mass, damping and stiffness matrices $[M]$, $[C]$ and $[K]$ are calculated using 4-node Mindlin-Reissner plate elements [19]. A surface spline was used to couple the structural and aerodynamic deflection degrees of freedom [20]. Due to the nature of the wing model, the structural and aerodynamic meshes overlap, though more structural than doublet-lattice elements are needed to model the plate deformation (typically an order of magnitude more). Plate thickness is defined at the nodes and will, as a result of the optimization, take on either a minimum or maximum value, such that a binary thickness distribution is obtained.

In order to solve Eq. 1, we utilize mode-reduction and a non-iterative frequency sweep method [21], whereby aerodynamic matrices $[Q(k)]$ are computed at pre-determined k values and linearly-interpolated between. One notable characteristic of this method is that the number of aeroelastic vibration modes (solutions to Eq. (1)) can change between airspeeds. In some cases, this is due to bifurcation or coalescence of modes (such as the formation of two equally-valid divergence modes), though in many cases, it is simply that a given mode frequency drifts either in or out of the range chosen for the sweep (such is discussed further in Section V). In this way, as will be seen in Section V, modes become present mid-way through the airspeed range. The entire solution procedure was completed via an in-house c++ code, which was developed and benchmarked against

Table 1: Benchmark Result Comparison with Attar et al. [22]

	Modal Freq. (Hz)					Flutter Characteristics	
	Mode 1	Mode 2	Mode 3	Mode 4	Mode 5	Speed (m/s)	Freq. (Hz)
Attar et al. (Theoretical)	7.54	30.00	34.58	71.35	86.18	42.8	23.1
Attar et al. (Experimental)	7.50	29.26	33.37	68.03	84.54	47.8	22.45
This Work	7.52	29.75	32.99	71.61	77.49	42.0	21.9

results from ASTROS [4] and experimental data [22].

For the sake of completeness, we include one set of validation results here. Table 1 compares modal frequencies and flutter characteristics obtained using the C++ code developed in this work with the theoretical and experimental values reported by Attar et al. [22] for a Lucite delta wing. It is considered that the general agreement shown, in addition to numerous comparisons performed in-house with the ASTROS [4] program, provides sufficient confidence in the code used herein.

The aeroelastic stability information is contained within the (non-dimensional) eigenvalues $p \equiv \gamma + ik$: A negative damping term ($\gamma < 0$) implies stability and vice versa. Flutter-like ($k > 0$) and divergence-like ($k = 0$) modes can be distinguished from the value of the corresponding reduced frequency k.

III. Optimization Method

With the aim to optimize the plate thickness distribution within a given wing planform, we require a method to define geometric boundaries (i.e. the boundary between thin and thick sections of plate) and track the movement of such through design iterations; this can be achieved efficiently via the use of the level set method [23, 24]. Developed originally for fluid interface tracking, the method has since found use in topology optimization as a way to define structural boundaries [25, 26]. Physical properties, in our case plate thickness h, can be mapped through the use of a scalar field ϕ, defined everywhere in the planform such that

$$h = h_0 + (h_1 - h_0)\ H(\phi) \tag{2}$$

where $H(.)$ is the Heaviside operator. In this way, plate thickness at a given position may assume

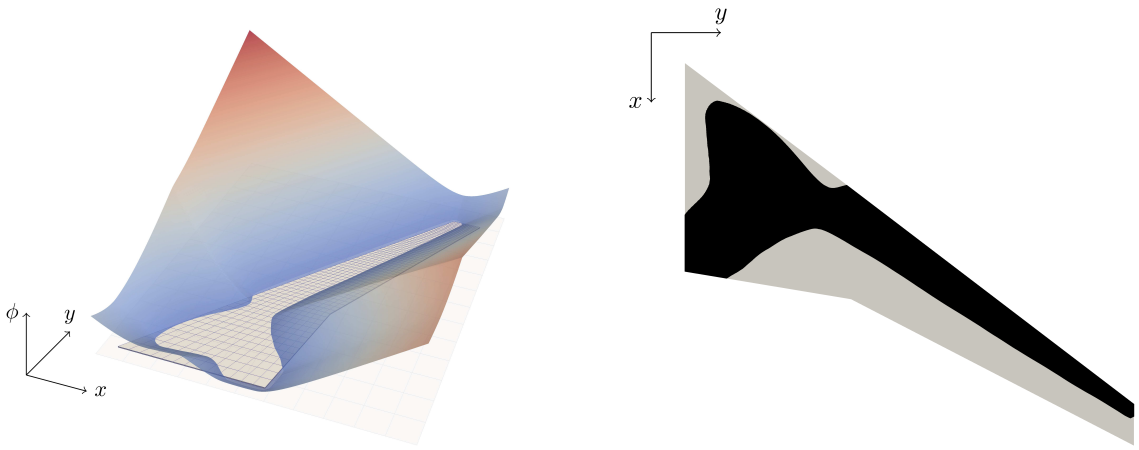

(a) Example ϕ field.

(b) Resulting plate thickness distribution.

Fig. 1: Wing structures are represented by the level set method.

only one of two distinct values: h_0 when $\phi < 0$ and h_1 when $\phi > 0$; the boundary is (implicitly) well-defined, occurring where $\phi = 0$. This concept is displayed graphically in Fig. 1.

The above implies a need to re-mesh the design at every iteration, such that the structural boundaries are well-represented in the flutter analysis. However from a practical standpoint, it is far more convenient to employ a fixed finite element mesh, the thickness values (though not geometry) of which are changed throughout the optimization, than to attempt re-meshing of arbitrary geometries. For this reason, a concession is often made to the above, such that a smooth Heaviside function is used instead [25]. In this work, we use

$$H(\phi) = \frac{1}{1 + e^{-s\phi}} \tag{3}$$

As such, the portion of structure nearest the boundary becomes "gray", taking-on intermediate thickness values. However, through judicious choice of the smoothing parameter s, we found the effect of the approximation on both global and local structural metrics to be negligible. Specifically, we chose s such that the vast majority of the smooth Heaviside curve occurred over the length of two plate elements. It is common-practice to maintain ϕ as a signed-distance function, such that $|\nabla\phi| = 1$ everywhere in the computational domain; this ensures a well-behaved boundary, both in terms of percentage gray elements and merging/splitting behavior. In this way, the entire ϕ field is not free to change arbitrarily; rather, at a given iteration, changes at the boundary points $\{\Delta\phi_b\}$

are propagated to changes at the level set grid nodes $\{\Delta\phi\}$ via the relation:

$$\{\Delta\phi\} = \left[\frac{\partial\phi}{\partial\phi_b}\right]\{\Delta\phi_b\} \tag{4}$$

The requirement that $|\nabla\phi| = 1$ everywhere allows the relational matrix $\left[\frac{\partial\phi}{\partial\phi_b}\right]$ to be computed. In order to achieve this, we use the fast marching algorithm [27]. It is noted that this procedure differs from the traditional level set method, whereby a velocity normal to the boundary is propagated to the remainder of the field via the Hamilton-Jacobi equation. The difference arises via use of the smooth Heaviside, which makes it possible to work with changes in ϕ directly.

The optimization procedure can be summarized as follows: We begin by choosing an initial design and the accompanying ϕ field; thickness is then assigned to each plate element via Eq. (2) and flutter analysis is carried out; once complete, the sensitivity of the objective and constraints are computed (details in Section IV), first with respect to the physical plate thickness, then to the ϕ field via Eq. (2), then to the boundary points via Eq. (4); lastly, we employ `IPOPT` [28] to select the optimal change in the ϕ field, thus updating the design, and repeat the process until convergence. In this way, the optimization problem is solved sequentially, with `IPOPT` used to solve a linearized sub-problem each iteration. More information regarding the sequential level set topology optimization can be found in Ref. [29].

IV. Application of Flutter & Divergence Constraints

The optimization problem is formulated as follows: For a given wing planform, choose the topology Ω (i.e. plate thickness distribution) which minimizes the weight W, such that the critical speed, defined as the lesser of the flutter and divergence speeds, is greater than or equal to a given value, which is expressed as a fraction f_c of that of the reference (uniform, maximum-thickness) design $V_c^{\Omega_0}$. Mathematically, it can be written:

$$\min_{\Omega} W \text{ subject to } V_c \geq f_c\, V_c^{\Omega_0} \tag{5}$$

However, since a given planform can have both flutter and divergence modes (sometimes multiples of each), and the critical mode can alternate depending on the topology of said planform, the above formulation is not always continuous with respect to design changes [8]. There exists an

equivalent in terms of the flutter eigenvalues $p \equiv \gamma + ik$ which, as per previous discussion, contain the stability information directly: At a given airspeed, if the real part γ is negative, the wing is stable for that mode, and vice versa. Thus, an equivalent problem statement is:

$$\min_{\Omega} W \text{ subject to } \gamma_j < 0 \; \forall \; V \in \left[0, f_c \; V_c^{\Omega_0}\right] \tag{6}$$

where j denotes the mode number. The above would suggest applying constraints at every velocity $V \in \left[0, f_c \; V_c^{\Omega_0}\right]$. However, by considering the wing planforms and associated behavior on a case-by-case basis, we found it sufficient to apply the constraints at a modest number of fixed velocity points only; such is detailed in Section V. It is possible that for more complex wing geometries, a general method would be required. In such eventualities, the active set method could be employed, whereby a large set of sample points is taken initially, then reduced based on the value of the constraints prior to derivative calculation; such has been used in both frequency [8] and time domain-based [30] optimization.

It is worth noting that the problem formulation (6) is necessarily simplistic in order to facilitate study of the relation between weight and flutter/divergence phenomena. It is understood that realistic design problems would include other complexities not included here, such as stress, buckling and fatigue constraints. The development herein should thus be considered a potential complement to research that considers the other design criteria.

In order to optimize (6), we require derivatives of W and γ with respect to plate thickness, i.e. $W_{,h}$ and $\gamma_{,h}$. In this work, we compute W as

$$W = \frac{\{z\}^T \left[M(h)\right] \{z\} - W_{\min}}{W_{\max} - W_{\min}} \tag{7}$$

where the $\{z\}$ vector is 1 for the plate deflection degrees of freedom (in the z-direction) and 0 elsewhere. The values for $W_{\min}$ and $W_{\max}$ are computed using $[M(h_{\min})]$ and $\left[M(h_{\max})\right]$ respectively. In this way, W represents a fraction of the maximum planform weight. The W derivative with respect to plate thickness can be computed simply as

$$W_{,h} = \frac{\{z\}^T \left[M_{,h}\right] \{z\}}{W_{\max} - W_{\min}} \tag{8}$$

For the γ derivative, we apply the adjoint method to the flutter equation (1). Pre-multiplying

$[F]$ by an adjoint vector $\{\lambda\}$ gives:

$$\{\lambda\}^T[F]\{u\} = 0 \tag{9}$$

where the right-hand side is now zero in the scalar sense. Taking the derivative of (9) with respect to plate thickness h, we get:

$$\{\lambda_{,h}\}^T[F]\{u\} + \{\lambda\}^T[F]\{u_{,h}\} + \{\lambda\}^T[F_{,h}]\{u\} = 0 \tag{10}$$

Since, by Eq. (1), $[F]\{u\} = \{0\}$, the first term in (10) is zero. Now since $\{u_{,h}\}$ cannot be known for arbitrary design variable changes, we will choose $\{\lambda\}$ such that the second term is also zero:

$$\{\lambda\}^T[F] = \{0\}^T \tag{11}$$

The above is called the adjoint equation. We solve Eq. (11) and the original flutter equation (1) via mode-reduction, with the assumption that the structural deflection and adjoint variable can be expressed as a linear combination of bases: $\{u\} = [\Phi]\{\eta\}$, $\{\lambda\} = [\Phi]\{\mu\}$, where $[\Phi]$ is a matrix containing eigenvectors from the free-vibration system, herein solved using the `ARPACK` software [31]. The mode-reduced versions of Eqs. (1) and (11) are then:

$$[\Phi]^T[F][\Phi]\{\eta\} \equiv [\bar{F}]\{\eta\} = \{0\} \tag{12}$$

$$([\Phi]\{\mu\})^T[F][\Phi] \equiv \{\mu\}^T[\bar{F}] = \{0\}^T \tag{13}$$

The mode reduction procedure will invalidate the original equations (1) and (11), and thus introduce sensitivity errors, unless a sufficient number of modes are retained (included in $[\Phi]$) [30, 32]. By numerical experimentation, we found 10 modes to be adequate for the range of wing planforms considered in Section V: For each reference design, incorporating more than 10 modes changed the predicted critical speed by less than 1%. In this work, Eqs. (12) and (13) were solved using `LAPACK` routines [33]. The derivative equation (10) then becomes

$$\{\lambda\}^T[F_{,h}]\{u\} = 0 \tag{14}$$

The matrix $[F_{,h}]$ contains terms which can be used to relate topological changes $[M_{,h}]$, $[C_{,h}]$, $[K_{,h}]$ to changes in the flutter eigenvalues $p_{,h} = \gamma_{,h} + ik_{,h}$. Namely, the above can be written

explicitly as

$$\gamma_{,h}\ \{\lambda\}^T \left[\left(\frac{2V}{c}\right)^2 2pM + \left(\frac{2V}{c}\right) C - \frac{q}{k}\ Q'' \right] \{u\}$$
$$+k_{,h}\ \{\lambda\}^T \left[\left(\frac{2V}{c}\right)^2 2ipM + \left(\frac{2V}{c}\right) iC - i\frac{q}{k}\ Q'' + p\frac{q}{k^2}\ Q'' - p\frac{q}{k}\ Q''_{,k} - q\ Q'_{,k} \right] \{u\}$$
$$+\{\lambda\}^T \left[\left(\frac{2V}{c}\right)^2 p^2 M_{,h} + \left(\frac{2V}{c}\right) pC_{,h} + K_{,h} \right] \{u\} = 0 \tag{15}$$

The real and imaginary parts of (15) can be used to solve for $\gamma_{,h}$ in terms of topology changes $[M_{,h}], [K_{,h}], [C_{,h}]$. Namely, let

$$\alpha_1 = \{\lambda\}^T \left[\left(\frac{2V}{c}\right)^2 2pM + \left(\frac{2V}{c}\right) C - \frac{q}{k}\ Q'' \right] \{u\}$$
$$\alpha_2 = \{\lambda\}^T \left[\left(\frac{2V}{c}\right)^2 2ipM + \left(\frac{2V}{c}\right) iC - i\frac{q}{k}\ Q'' + p\frac{q}{k^2}\ Q'' - p\frac{q}{k}\ Q''_{,k} - q\ Q'_{,k} \right] \{u\}$$
$$\alpha_3 = \{\lambda\}^T \left[\left(\frac{2V}{c}\right)^2 p^2 M_{,h} + \left(\frac{2V}{c}\right) pC_{,h} + K_{,h} \right] \{u\}$$
$$\rightarrow \alpha_1 \gamma_{,h} + \alpha_2 k_{,h} + \alpha_3 = 0$$

Then we can write:

$$\alpha'_1 \gamma_{,h} + \alpha'_2 k_{,h} + \alpha'_3 = 0$$
$$\alpha''_1 \gamma_{,h} + \alpha''_2 k_{,h} + \alpha''_3 = 0$$

which can be solved simultaneously:

$$\rightarrow \left(\alpha'_1 - \frac{\alpha'_2}{\alpha''_2} \alpha''_1 \right) \gamma_{,h} = \left(\frac{\alpha'_2}{\alpha''_2} \alpha''_3 - \alpha'_3 \right) \tag{16}$$

The above analytical expression for $\gamma_{,h}$ has been checked against central finite difference results for a range of representative configurations. One example is shown in Fig. 2, which is for the unswept reference planform from Fig. 4a at 25 m/s; samples were taken at each of the FEA nodes. As per later discussion, this design point includes information from several flutter modes, one of which is unstable, as well as two divergence modes. There was no apparent trend regarding mode type and error distribution. It is worth noting that these errors arise from two sources: the first is due to the first derivative truncation itself, and the other is the approximation introduced via mode reduction. As depicted in Fig. 2, there is a significant reduction in error when 10 modes are retained in the

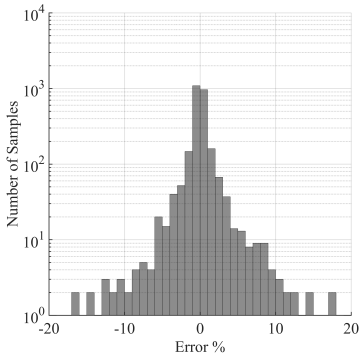

(a) 5 modes retained; mean = 0.03%, std = 2.12%.

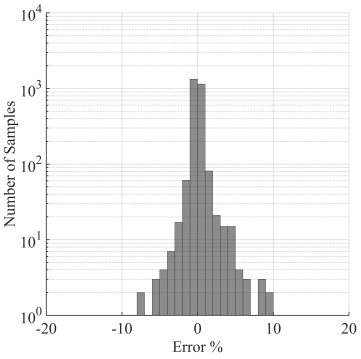

(b) 10 modes retained; mean = 0.06%, std = 0.92%.

Fig. 2: Comparison between finite difference and analytical γ derivatives.

flutter analysis compared to 5, though additional modes yielded far less improvement, and incur significant computational cost.

Once derivatives with respect to h are computed, it is straightforward to transform them to the level set field ϕ, and to the movement of the boundary points, via Eqs. (2) and (4).

V. Results

In each of the results that follow, the wing material comprises an aluminum plate with a mean chord of 0.3m, to be optimized for thickness distributions of 0.5 and 1.5 mm, represented in the figures by gray and black regions on the planforms, respectively; structural damping is assumed negligible. The wing structures are clamped at zero angle of attack along the entire root edge (left-most edge in the figures), which marks the aerodynamic symmetry plane. Dynamic pressure is calculated using sea-level air density at zero Mach number. Such dimensions and flight conditions were chosen to facilitate a comparison with the previously-published work [13]. It is worth noting that a non-zero minimum plate thickness avoids issues arising from highly-localized vibration mode formation [34].

The number of chord-wise finite elements was on the order of 100, with as many as required span-wise in order to approximately maintain unit aspect ratios (thus high quality elements). This number was found to be large enough such that several finite elements remained present on any structural features which formed in the optimized design, thus retaining accuracy in the fixed grid

(a) Representative aerodynamic mesh.

(b) Representative structural mesh.

Fig. 3: Representative meshes used

simulation method utilized. The number of chord-wise doublet lattice elements was on the order of 10, again, with as many required span-wise to maintain approximate unit aspect ratios. As discussed by Rodden et al. [18], the maximum k value which can be accurately simulated in Eq. (1) is dictated by the ratio of chord length to the number of chord-wise elements. The number of chord-wise elements chosen here allowed k values between 0 and 2.25 to be simulated, which we found high-enough to capture the flutter and divergence behavior relevant to this study. That is to say, any solutions to Eq. (1) with k values outside this range did not impact the flutter or divergence speeds recorded herein. Accordingly, the results which follow can only include solutions to Eq. (1) with k values in this range. This accounts for modes becoming present mid-way through the velocity range shown in the figures, since when absent, those modes have k values outside the range permitted by the aerodynamic mesh used, and cannot be simulated accurately. For all planforms shown, we used 100 k values to pre-compute the aerodynamic $[Q(k)]$ matrices; 20 matrices were uniformly sampled between 0 and 0.1, the remainder were uniformly sampled between 0.1 and 2.25. This scheme was chosen based on experience: solutions tend to have higher stability (in terms of smoothness between velocities) when a cluster of k values close to zero is used. Sample aerodynamic and structural meshes are depicted in Fig. 3.

The first result is that of an unswept aspect ratio (AR) 6 planform shown in Fig. 4. The reference (i.e. uniform, 1.5 mm thick) design is flutter-critical at 23 m/s; divergence occurs at 28 m/s. The design shown in Fig. 4b was obtained through optimization with $f_c = 1.0$ from Eq. (6); that is, weight is minimized subject to no reduction in the critical speed. Accordingly, the optimized design

shares the same 23 m/s critical speed as the reference, though now both flutter and divergence occur at this point. The weight W (i.e. proportion of planform filled by maximum-thickness plate) has reduced by 73% compared to the reference design. Since, for this type of planform, the damping terms γ_j tend to be monotonic functions of the airspeed, we found it necessary to implement the aeroelastic constraints (Eq. (6)) at the maximum speed (i.e. 23 m/s) only.

Convergence for this planform, as well as all those subsequent, was deemed to occur when all constraints were satisfied and weight reduced by less than 0.1% in 10 iterations. Fig. 4g depicts the weight (in red) and constrained damping values (in black) throughout the design iterations. The starting design was, as for all planforms considered, the reference design i.e. planform filled with maximum thickness plate. Several alternative starting designs were also tried, however each converged to topologies remarkably similar to those shown, with the same overall and functional features.

As for the topological features, two are prominent: A forward shift in both the flexural axis and center of gravity, and a stiffening member towards the trailing edge of the root; such features complement both intuition and idealized results. Namely, it can be shown that flexible wing divergence will not occur given the flexural axis is far enough forward with respect to the aerodynamic center (c.f. section 8.2 of reference [35]). Moreover, forward shifting the center of gravity (known as mass balancing) is a well-known flutter prevention strategy [13, 36]. It is worth noting, however, that we found both mass and stiffness to be salient: A significant weight penalty must be paid if one is to attempt flutter control using mass distribution only. This idea will be exemplified for the CRM planform later in this section.

The role of the stiffening member near the trailing edge root can be examined by removing it and analyzing the resulting design. Upon doing this, we observed that the difference between the first (bending) and second (twisting) natural frequencies of the design reduced by 10%, as did the flutter speed. Frequency separation is known to delay the coalescence of the first two aeroelastic modes [13], and has been used as a proxy for flutter performance in the past [37]; the stiffening member thus appears to be acting in this capacity. In contrast, the thicker skin nearest the leading edge root pertains to divergence control: Removing it caused the divergence speed to fall drastically,

(a) Reference design thickness distribution;

$V_f = 23$, $V_d = 28$ m/s; W = 100%.

(b) Optimized design thickness distribution;

$V_f = V_d = 23$ m/s; W = 27%.

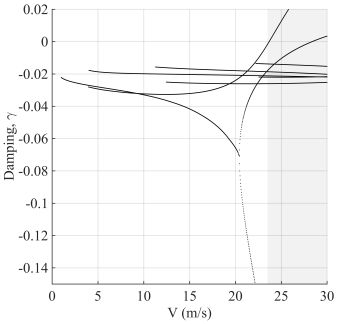

(c) Reference design damping

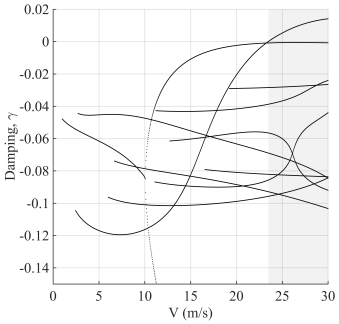

(d) Optimized design damping

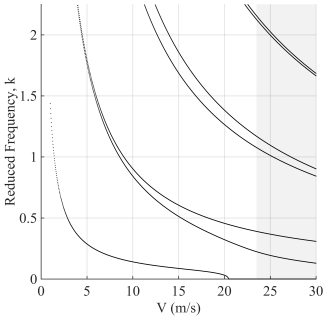

(e) Reference design frequency

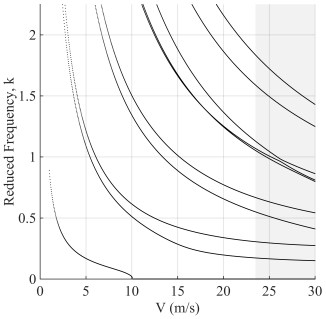

(f) Optimized design frequency

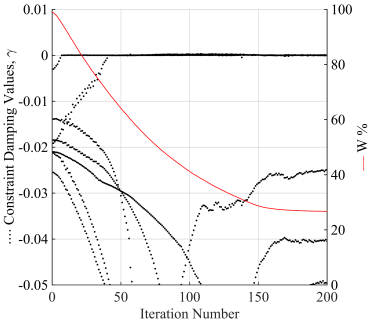

(g) Convergence history

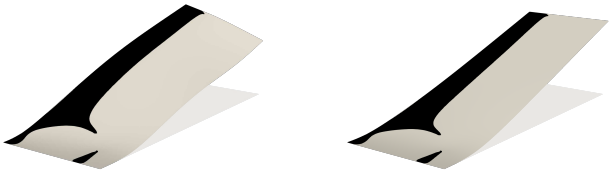

(h) Flutter (left) and divergence (right) mode shapes

Fig. 4: Results for unswept AR = 6 wing.

while the flutter speed actually improved.

The optimum solutions for higher aspect ratio planforms retained essentially the same structural

features: Fig. 5 shows an example where AR = 30. Despite being much lower in value, the flutter and divergence speeds converged and a similar weight reduction was achieved. It has been suggested that geometric nonlinearity should be included in such high AR simulations [38, 39]; such will be considered in future work, for situations where the wing flutters about a deformed configuration.

The effect of sweep angle is explored in Figs. 6 and 7, wherein 20° back- and forward-swept planforms have been optimized. In order to control the hump modes in the γ curves for the swept planforms, we required constraints on 5 equally spaced sample velocities in the $0 - 30$ m/s range. As expected, the back-swept reference design is flutter critical, and does not register a divergence speed. In contrast, the optimal design does diverge, though this occurs at a higher speed than that of flutter. There is, then, less pressure on the topology to control divergence than there is flutter. Such can explain the observed topological features: the optimal design forward shifts the flexural axis and center of gravity as per the unswept planform. However, the stiffening closest to the leading edge root has vanished; as per the observations made for the unswept planform above, this area pertains mainly to divergence control, which is not critical for this planform. The trailing edge stiffening has also atrophied. By the previous analysis on the unswept planform, the trailing edge structure appeared to be acting to reduce bend-twist coupling and increase flutter speed. However, compared to an unswept planform of equal weight, the back-swept planform is naturally more flutter resistant. It seems, then, that the backswept structure was able to reach an optimum design point without requiring this mechanism.

In contrast, the reference forward-swept planform is initially divergence critical. Post-optimization, the flutter and divergence speeds are matched at 14 m/s, and the divergence mode has become notably hump-shaped, touching the stability axis at the constraint speed; such control of the divergence behavior has required the notable presence of leading edge root stiffening. The lack of stiffening at the trailing edge root, and indeed less material overall compared to the previous

(a) Optimized design thickness distribution; $V_f = 3.5$, $V_d = 3.5$ m/s; $W = 28\%$.

Fig. 5: Results for the unswept AR = 30 wing

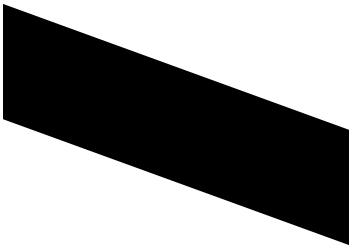

(a) Reference design thickness distribution;

$V_f = 21$, $V_d > 30$ m/s; W = 100%.

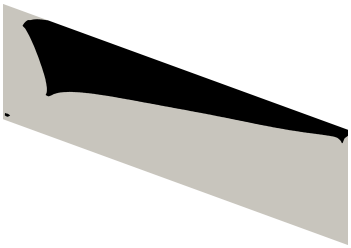

(b) Optimized design thickness distribution;

$V_f = 21$, $V_d = 24$ m/s; W = 31%.

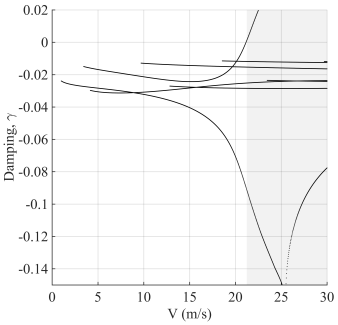

(c) Reference design damping

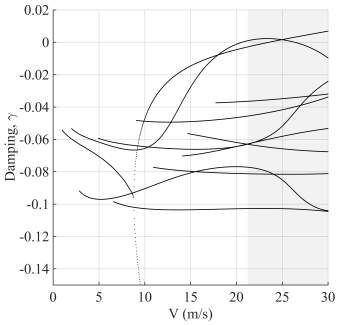

(d) Optimized design damping

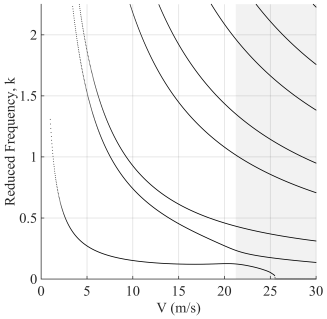

(e) Reference design frequency

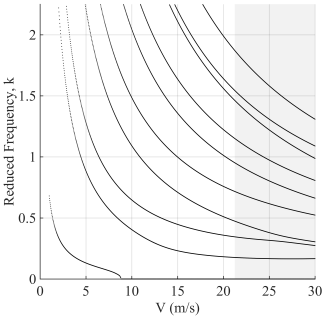

(f) Optimized design frequency

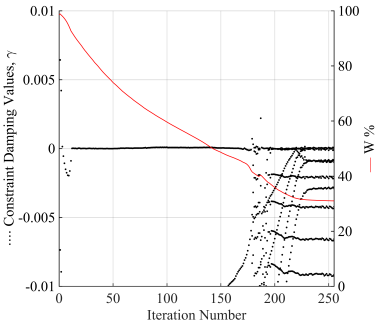

(g) Convergence history

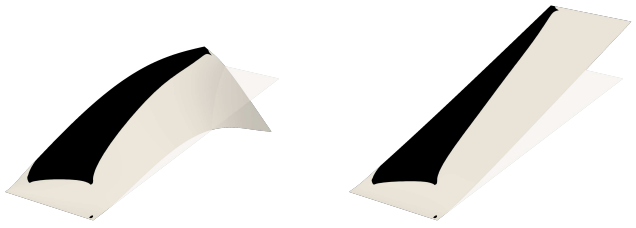

(h) Flutter (left) and divergence (right) mode shapes

Fig. 6: Results for backswept AR = 6 wing.

planforms can be explained, since the flutter speed, which requires the mass balancing and trailing edge root stiffening, has been allowed to reduce significantly compared to the reference.

It is worth noting that the divergence mode damping plots tend to be quite flat in relation to velocity, such that the optimized designs have divergence γ values close to zero over a wide velocity range; such is especially noticeable in Fig. 7d. Accordingly, the divergence speeds reported herein can be said to be very sensitive to design changes. Such will also be true of the flutter speed in planforms studied later in this article. This, however, can be addressed in the optimization problem formulation: Herein, we simply require $\gamma < 0$, though in practice, one could apply the constraint at some safety margin, requiring $\gamma \ll 0$ etc., though such would be expected to incur significant weight penalties.

As noted above, these rectangular planforms have been subjected to optimization previously by Stanford and Beran [13]. One key difference between that and the present work is that the former formulated an unconstrained optimization problem: A weighted sum of the wing mass and critical speed was used as the objective, which was then minimized and a Pareto front presented; this work minimized mass subject to constraints on the critical speed (via the eigenvalues). This difference notwithstanding, the topological features presented for the optimal designs in Ref. [13] and those shown above are remarkably similar: The observations pertaining to the flexural axis forward-shift and root stiffening could be applied equally to both works, and we consider this to validate our methodology. A quantitative comparison can be made for only some of the results in Ref. [13], namely those where the critical speed is exactly maintained (since this approximates our formulation). In these cases, we report far lower optimal wing masses: The equivalent designs for Figs. 4, 6 and 7 given in Ref. [13] had weights approximately 35, 40 and 20%. The primary reason for this improvement is considered to arise from the chosen optimization methodology. Stanford and Beran [13] employed a SIMP (Solid Isotropic Material with Penalization) topology optimization algorithm [40], which struggled to obtain binary designs; in such algorithms, intermediate (gray) elements are allowed to persist throughout the optimization, though are penalized such that binary designs tend to emerge. Indeed, an explicit density penalty was added to force binary designs in Ref. [13], which inevitably leads to some loss of performance. Such can clearly be observed in the

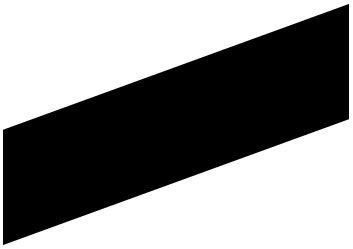

(a) Reference design thickness distribution;

$V_f = 28$, $V_d = 14$ m/s; W = 100%.

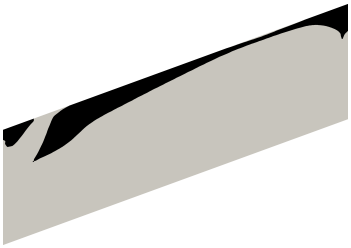

(b) Optimized design thickness distribution;

$V_f = 14$, $V_d = 14$ m/s; W = 13%.

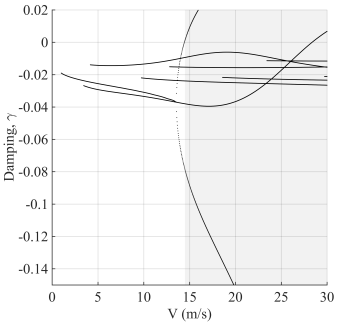

(c) Reference design damping

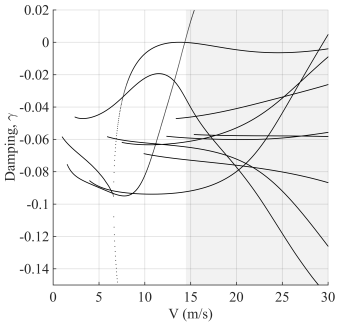

(d) Optimized design damping

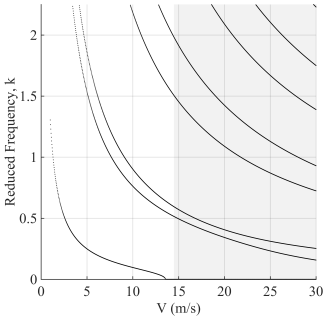

(e) Reference design frequency

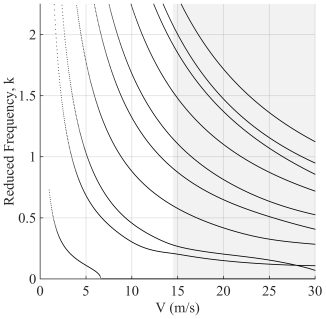

(f) Optimized design frequency

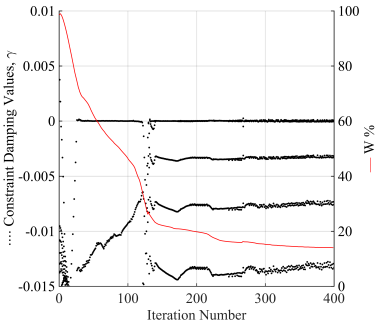

(g) Convergence history

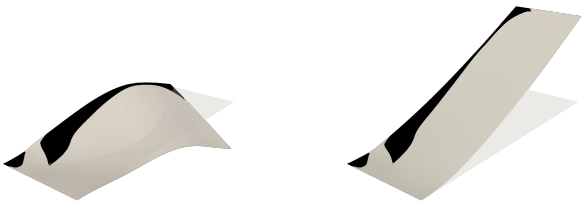

(h) Flutter (left) and divergence (right) mode shapes

Fig. 7: Results for forwardswept AR = 6 wing.

convergence histories, e.g. Fig. 4 of Ref. [13]: when the explicit penalty is applied, a visible drop in performance follows. Furthermore, the final designs, e.g. Fig. 6 of Ref. [13], display checkerboarding, whereby adjacent elements oscillate between thick and thin material. Such is unlikely to be an optimum phenomenon, and is considered more likely to be an inefficiency introduced by the penalty terms.

A more exotic topology was retrieved upon consideration of a 45^o, 0.6 m root chord delta wing planform clipped at 95% span, as shown in Fig. 8b. Accompanying the marked 94% weight-reduction are several constrained hump flutter modes as per Fig. 8d. In order to attain this degree of control over the γ_j, we required 20 equally-spaced constraint velocities. As above, in order to ascertain the role of each retrieved topological feature, we removed each individually and analyzed the behavior; these results are shown in Fig. 9. As each feature is removed, it can be seen from the corresponding damping curves that one or two modes become unstable, while the others remain largely controlled. We submit this behavior to be unintuitive and complex, highlighting the ability of the proposed method to uncover useful design strategies previously unknown.

The last planform considered is that of the common research model (CRM) planform [41] as shown in Fig. 10. The wing was scaled in order to have a mean chord of 0.3 m. Akin to the delta wing, hump flutter modes are present in the damping plots of the optimized design, and we again required constraints at 20 equally-spaced velocities in the range shown. This planform does not have a divergence speed, and akin to the backswept planform discussed above, employs a forward-shifted flexural axis and center of gravity, though no root or trailing edge stiffening remains.

We also utilized this planform to investigate the effect that mass and stiffness in the maximum-thickness plate have on flutter control. This planform is most appropriate of all considered since as mentioned, the CRM does not register a divergence speed in the velocity range; flutter behavior can thus be studied in isolation. It is worth noting that under the simulation method utilized here, the mass matrix cannot affect the divergence speed (at divergence, $p = 0 + 0i$ and $[M]$ drops-out of the flutter equation (1)). We proceeded to undertake a weight minimization problem in two ways: the first assigned structural stiffness and mass matrices according to the plate thickness distribution as for all cases above; the second only assigned mass matrices according to the thickness

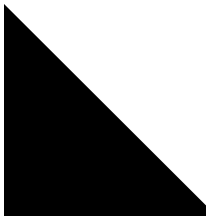

(a) Reference design thickness distribution;

$V_f = 62$, $V_d > 70$ m/s; W = 100%.

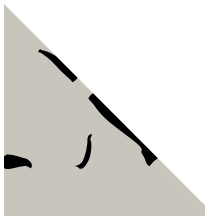

(b) Optimized design thickness distribution;

$V_f = 62$, $V_d > 70$ m/s; W = 6.4%.

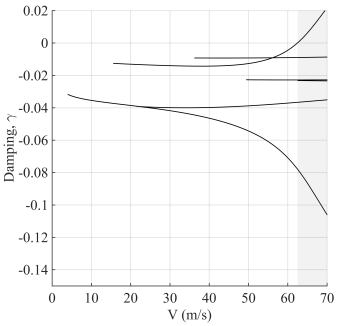

(c) Reference design damping

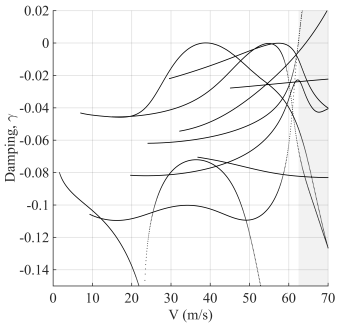

(d) Optimized design damping

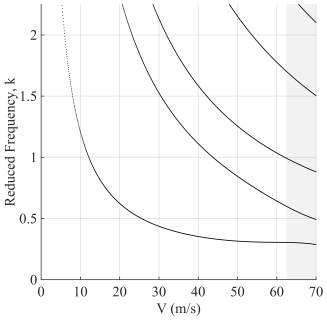

(e) Reference design frequency

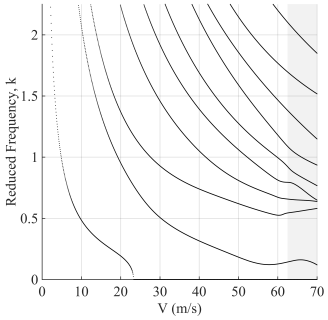

(f) Optimized design frequency

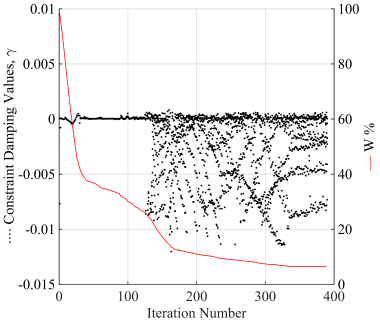

(g) Convergence history

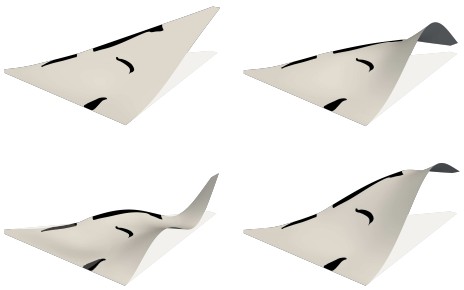

(h) Flutter mode shapes at 39 (upp. left), 55 (upp. right), 58 (low. left) and 62 (low. right) m/s.

Fig. 8: Results for Delta wing.

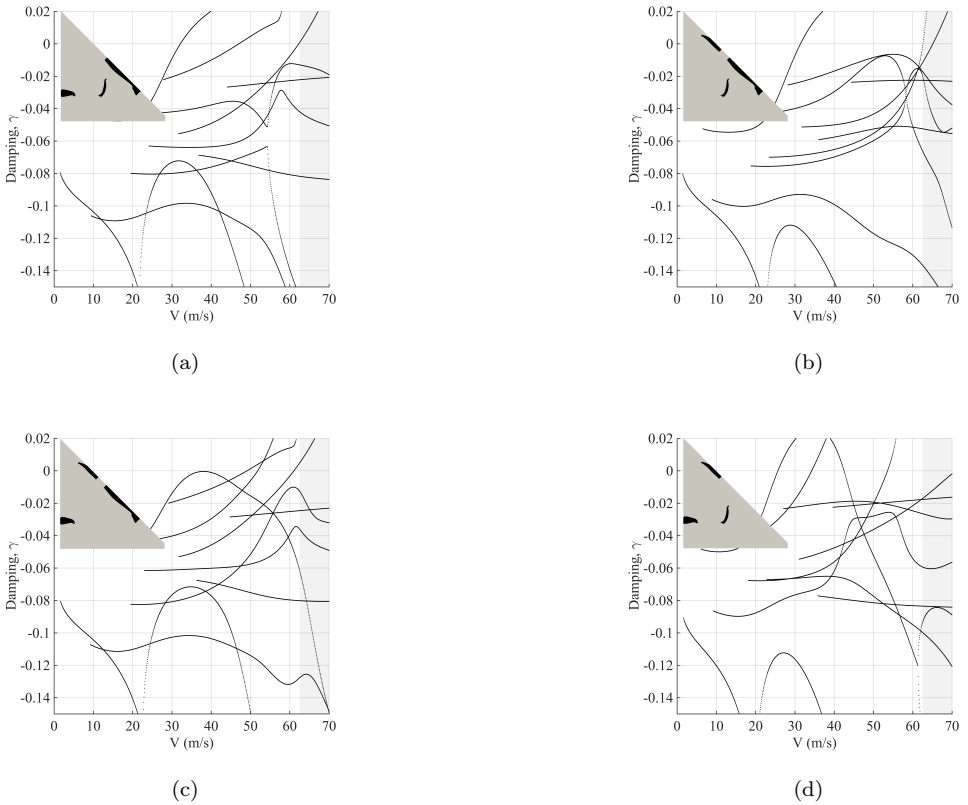

Fig. 9: By removing one topological feature at a time, its role in flutter prevention is visualized.

distribution, while retaining the stiffness matrices from the minimum thickness plate. This situation thus simulates adding non-structural mass to the planform in order to control flutter. The constraint was set such that no flutter could occur prior to 8.5 m/s; higher flutter speeds could not be obtained using mass distribution only.

The results are depicted in Fig. 11. While both designs have equal flutter speeds, more than 40% more weight is required by the design utilizing mass distribution only. It is therefore considered that the mass-balancing effect observed in the optimized designs above is not sufficient in itself to provide low-weight, flutter-controlled wing structures. Also salient is the stiffness in the maximum thickness plate, and the accompanying changes in flexural axis.

Lastly, in order to demonstrate the ability of the proposed method to not only maintain, but indeed increase critical speed while reducing weight, the CRM planform was optimized using $f_c =$ 1.5 and 2.0; that is, minimize mass subject to 50% increase and 100% increase in critical speed

(a) Reference design thickness distribution;

$V_f = 21$, $V_d > 30$ m/s; W = 100%.

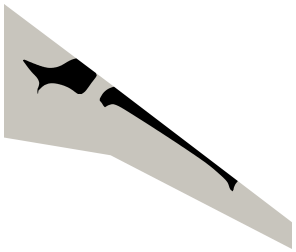

(b) Optimized design thickness distribution;

$V_f = 21$, $V_d > 30$ m/s; W = 14%.

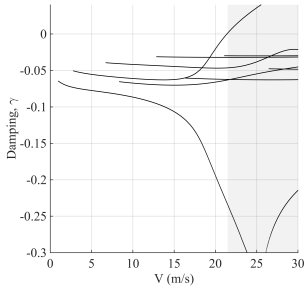

(c) Reference design damping

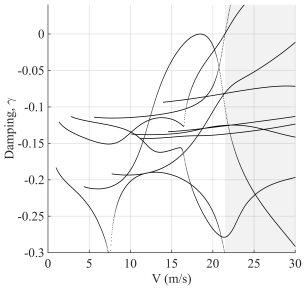

(d) Optimized design damping

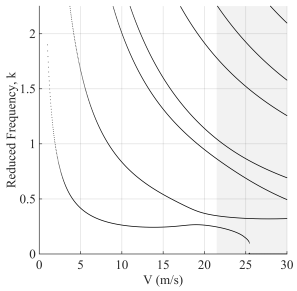

(e) Reference design frequency

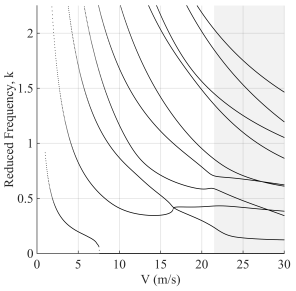

(f) Optimized design frequency

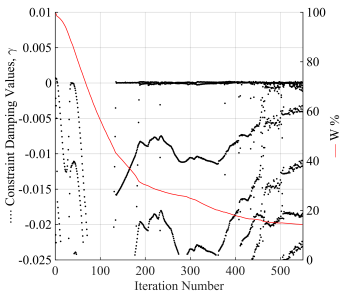

(g) Convergence history

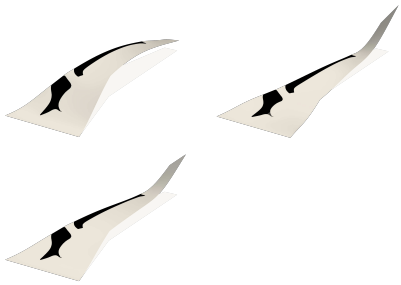

(h) Flutter mode shapes at 18 (upp. left) and 21 (upp. right and low. left) m/s.

Fig. 10: Results for CRM wing.

respectively. As shown in Fig. 12, even when the critical speed was required to double (Fig. 12b),

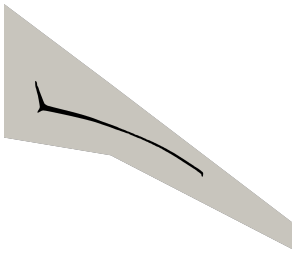

(a) Stiffness and mass distribution;
$V_f = 8.5$, $V_d > 45$ m/s; $W = 4.0\%$.

(b) Mass distribution only;
$V_f = 8.5$, $V_d > 45$ m/s; $W = 46\%$.

Fig. 11: Influence of mass and stiffness distribution

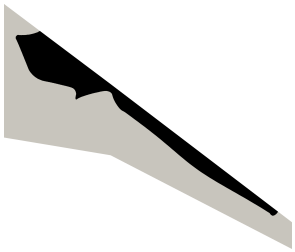

(a) Optimized design with $f_c = 1.5$;
$V_f = 32$, $V_d > 45$ m/s; $W = 27\%$.

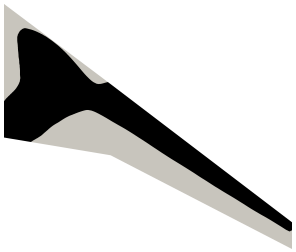

(b) Optimized design with $f_c = 2.0$;
$V_f = 42$, $V_d = 43$ m/s; $W = 56\%$.

Fig. 12: Increasing flutter speed of CRM planform.

weight is was still reduced to 56% with respect to the reference.

VI. Conclusions

This article demonstrates an application of the level set method to the structural topology optimization of plate-like wings under flutter and divergence constraints. It is shown that applying said constraints on the eigenvalues of the flutter equation results in a robust design strategy, capable of significantly reducing weight while maintaining or increasing flutter and/or divergence speed. The optimum solutions obtained for the rectangular planforms are explicable in terms of known aeroelastic phenomena, comprised the features identified by the previous works, and allowed significantly more weight reduction. Moreover, the extension to the CRM and delta planforms, where multiple flutter modes must be simultaneously controlled, demonstrated the versatility of the proposed method. The strategy can offer new insights into optimal aeroelastic wing structures, and

could be used to complement research that considers other relevant design criteria (stress, buckling, fatigue etc.). Future work will incorporate these other relevant constraints, as well as more realistic 3D wing geometries.

Acknowledgments

We acknowledge the support of the Engineering and Physical Sciences Research Council, Fellowship for Growth grant EP/M002322/2. We would also like to thank the Numerical Analysis Group at the Rutherford Appleton Laboratory for their FORTRAN HSL packages (HSL, a collection of Fortran codes for large-scale scientific computation).

References

[1] Thomas Binder, Peter Hougardy, and Peter Haffner. Optimization of castings and forgings at audi ag. *Simulation-das Fachmagazin fuer FEM, CFD und MKS*, 2003.

[2] Michael H Shirk, Terrence J Hertz, and T Weisshaar. Aeroelastic tailoring-theory, practice, and promise. *Journal of Aircraft*, 23(1):6–18, 1986. doi:10.2514/3.45260.

[3] LA McCullers and RW Lynch. Dynamic characteristics of advanced filamentary composite structures. *Volumes I through III, AFFDL-TR-73-111, Air Force Flight Dynamics Laboratory, Wright-Patterson AFB, Ohio*, 1974.

[4] DJ Neill, DL Herendeen, and VB Venkayya. Astros enhancements: Volume iii-astros theoretical manual. *Flight Dynamics Directorate, Wright Laboratory, Wright Patterson Air Force Base, WL-TR-95-3006*, 1995.

[5] Raphael T Haftka. Parametric constraints with application to optimization for flutter using a continuous flutter constraint. *AIAA Journal*, 13(4):471–475, 1975. doi:10.2514/3.49733.

[6] W Jefferson Stroud, T Krishnamurthy, Brian H Mason, Steven A Smith, and Ahmad S Naser. Probabilistic design of a plate-like wing to meet flutter and strength requirements. In *Proceedings of AIAA Structures, Structural Dynamics, and Materials Conference, Denver, CO*, 2002. doi:10.2514/6.2002-1464.

[7] Y Odaka and H Furuya. Robust structural optimization of plate wing corresponding to bifurcation in higher mode flutter. *Structural and Multidisciplinary Optimization*, 30(6):437–446, 2005. doi:10.1007/s00158-005-0538-9.

[8] UT Ringertz. On structural optimization with aeroelasticity constraints. *Structural and Multidisciplinary Optimization*, 8(1):16–23, 1994. doi:10.1007/BF01742928.

[9] Christine V Jutte, Bret K Stanford, Carol D Wieseman, and James B Moore. Aeroelastic tailoring of the nasa common research model via novel material and structural configurations. In *AIAA SciTech Conference*, pages 13–17. AIAA Reston, VA, 2014. doi:10.2514/6.2014-0598.

[10] JKS Dillinger, Thomas Klimmek, Mostafa M Abdalla, and Zafer Gürdal. Stiffness optimization of composite wings with aeroelastic constraints. *Journal of Aircraft*, 2013. doi:10.2514/1.C032084.

[11] Masaki Kameyama and Hisao Fukunaga. Optimum design of composite plate wings for aeroelastic characteristics using lamination parameters. *Computers & structures*, 85(3):213–224, 2007. doi:10.1016/j.compstruc.2006.08.051.

[12] Peter D Dunning, Bret K Stanford, H Alicia Kim, and Christine V Jutte. Aeroelastic tailoring of a plate wing with functionally graded materials. *Journal of Fluids and Structures*, 51:292–312, 2014. doi:10.1016/j.jfluidstructs.2014.09.008.

[13] Bret Stanford and Philip Beran. Optimal structural topology of a platelike wing for subsonic aeroelastic stability. *Journal of Aircraft*, 48(4):1193–1203, 2011. doi:10.2514/1.C031185.

[14] Bret K Stanford and Peter D Dunning. Optimal topology of aircraft rib and spar structures under aeroelastic loads. *Journal of Aircraft*, 2014. doi:10.2514/1.C032913.

[15] Peter D Dunning, Bret K Stanford, and H Alicia Kim. Level-set topology optimization with aeroelastic constraints. In *AIAA SciTech Conference*, pages 5–9, 2015. doi:10.2514/6.2015-1128.

[16] K Maute and M Allen. Conceptual design of aeroelastic structures by topology optimization. *Structural and Multidisciplinary Optimization*, 27(1):27–42, 2004. doi:10.1007/s00158-003-0362-z.

[17] Hermann J Hassig. An approximate true damping solution of the flutter equation by determinant iteration. *Journal of Aircraft*, 8(11):885–889, 1971. doi:10.2514/3.44311.

[18] William P Rodden, Paul F Taylor, and Samuel C McIntosh. Further refinement of the subsonic doublet-lattice method. *Journal of Aircraft*, 35(5):720–727, 1998. doi:10.2514/2.2382.

[19] Klaus-Jürgen Bathe and Eduardo N Dvorkin. A four-node plate bending element based on mindlin/reissner plate theory and a mixed interpolation. *International Journal for Numerical Methods in Engineering*, 21(2):367–383, 1985. doi:10.1002/nme.1620210213.

[20] Robert L Harder and Robert N Desmarais. Interpolation using surface splines. *Journal of aircraft*, 9(2):189–191, 1972. doi:10.2514/3.44330.

[21] Louw H van Zyl. Aeroelastic divergence and aerodynamic lag roots. *Journal of aircraft*, 38(3):586–588, 2001. doi:10.2514/2.2806.

[22] PJ Attar, EH Dowell, and DM Tang. A theoretical and experimental investigation of the effects of a steady angle of attack on the nonlinear flutter of a delta wing plate model. *Journal of Fluids and Structures*, 17(2):243–259, 2003. doi:10.1016/S0889-9746(02)00123-8.

[23] James Albert Sethian. *Level set methods and fast marching methods: evolving interfaces in computational geometry, fluid mechanics, computer vision, and materials science*, volume 3. Cambridge university press, 1999.

[24] Stanley Osher and Ronald Fedkiw. *Level set methods and dynamic implicit surfaces*, volume 153. Springer Science & Business Media, 2006. doi:10.1007/b98879.

[25] Michael Yu Wang, Xiaoming Wang, and Dongming Guo. A level set method for structural topology optimization. *Computer methods in applied mechanics and engineering*, 192(1):227–246, 2003. doi:10.1016/S0045-7825(02)00559-5.

[26] Grégoire Allaire, François Jouve, and Anca-Maria Toader. Structural optimization using sensitivity analysis and a level-set method. *Journal of computational physics*, 194(1):363–393, 2004. doi:10.1016/j.jcp.2003.09.032.

[27] David Adalsteinsson and James A Sethian. The fast construction of extension velocities in level set methods. *Journal of Computational Physics*, 148(1):2–22, 1999. doi:10.1006/jcph.1998.6090.

[28] Andreas Wächter and Lorenz T Biegler. On the implementation of an interior-point filter line-search algorithm for large-scale nonlinear programming. *Mathematical programming*, 106(1):25–57, 2006. doi:10.1007/s10107-004-0559-y.

[29] Peter D Dunning and H Alicia Kim. Introducing the sequential linear programming level-set method for topology optimization. *Structural and Multidisciplinary Optimization*, 51(3):631–643, 2015. doi:10.1007/s00158-014-1174-z.

[30] Byung-Soo Kang, Gyung-Jin Park, and Jasbir S Arora. A review of optimization of structures subjected to transient loads. *Structural and Multidisciplinary Optimization*, 31(2):81–95, 2006. doi:10.1007/s00158-005-0575-4.

[31] Richard B Lehoucq, Danny C Sorensen, and Chao Yang. *ARPACK users' guide: solution of large-scale eigenvalue problems with implicitly restarted Arnoldi methods*. SIAM, 1998. doi:10.1137/1.9780898719628.

[32] AC Paul, A Dutta, and CV Ramakrishnan. Accurate computation of design sensitivities for dynamically loaded structures with displacement constraints. *AIAA journal*, 34(8), 1996. doi:10.2514/3.13288.

[33] Edward Anderson, Zhaojun Bai, Christian Bischof, L Susan Blackford, James Demmel, Jack Dongarra, Jeremy Du Croz, Anne Greenbaum, Sven Hammarling, Alan McKenney, et al. *LAPACK Users' guide*.

SIAM, 1999. doi:10.1137/1.9780898719604.

[34] Niels L Pedersen. Maximization of eigenvalues using topology optimization. *Structural and multidisciplinary optimization*, 20(1):2–11, 2000. doi:10.1007/s001580050130.

[35] Jan Robert Wright and Jonathan Edward Cooper. *Introduction to aircraft aeroelasticity and loads*, volume 20. John Wiley & Sons, 2008. doi:10.2514/4.479359.

[36] Raymond L Bisplinghoff, Holt Ashley, and Robert L Halfman. *Aeroelasticity*. Courier Corporation, 2013. doi:10.1002/zamm.19560360764.

[37] R Butler and JR Banerjee. Optimum design of bending-torsion coupled beams with frequency or aeroelastic constraints. *Computers & structures*, 60(5):715–724, 1996. 10.1016/0045-7949(95)00451-3.

[38] Mayuresh J Patil and Dewey H Hodges. On the importance of aerodynamic and structural geometrical nonlinearities in aeroelastic behavior of high-aspect-ratio wings. *Journal of Fluids and Structures*, 19(7):905–915, 2004. doi:10.1016/j.jfluidstructs.2004.04.012.

[39] DM Tang and EH Dowell. Effects of geometric structural nonlinearity on flutter and limit cycle oscillations of high-aspect-ratio wings. *Journal of fluids and structures*, 19(3):291–306, 2004. doi:10.1016/j.jfluidstructs.2003.10.007.

[40] Martin P Bendsøe, Ole Sigmund, Martin P Bendsøe, and Ole Sigmund. *Topology optimization by distribution of isotropic material*. Springer, 2004. doi:10.1007/978-3-662-05086-6_1.

[41] John C Vassberg, Mark A DeHaan, S Melissa Rivers, and Richard A Wahls. Development of a common research model for applied cfd validation studies. *AIAA paper*, 6919:2008, 2008. doi:10.2514/6.2008-6919.